Chapter 3

GW for surfaces and thin films

Plane-wave implementations of the DFT and *GW* schemes introduced in the previous chapter naturally assume three-dimensional periodicity. In this chapter we will describe how they can be used to model two-dimensional systems like thin films and surfaces by means of the "repeated-slab approach". We will address briefly how it performs for DFT ground-state calculations before coming to the main point of this chapter, the repeated-slab approach in *GW* calculations. We will first show that the assumption of isotropic screening leads to a numerical instability in *GW* calculations and how this can be overcome. We will then demonstrate that the long-range screening leads to a particular, slow convergence behaviour for the **k**-point sampling, which turns out to be one of the most critical parameters. The screening effects in a repeated slab system can be understood with a simple dielectric model. From this model, a robust correction scheme is derived that makes efficient *GW* calculations using the repeated-slab approach possible.

3.1 Repeated-slab approach

The use of plane-waves as basis set for DFT-KS and *GW* calculations implies a periodic repetition in all three spatial directions. This is naturally fulfilled for bulk crystals, but in two-dimensional systems like thin films or surfaces the periodicity is broken in one direction. To overcome this difficulty, a structural model for the surface is used that is compatible with three-dimensional periodic boundary conditions. In a first step, the semi-infinite substrate below the surface or the supported thin film is replaced by a finite slab. The thickness of this slab is an important (structural) convergence parameter. Then an artificial periodicity is introduced in the direction of the broken symmetry, i.e. perpendicular to the surface. This is schematically depicted

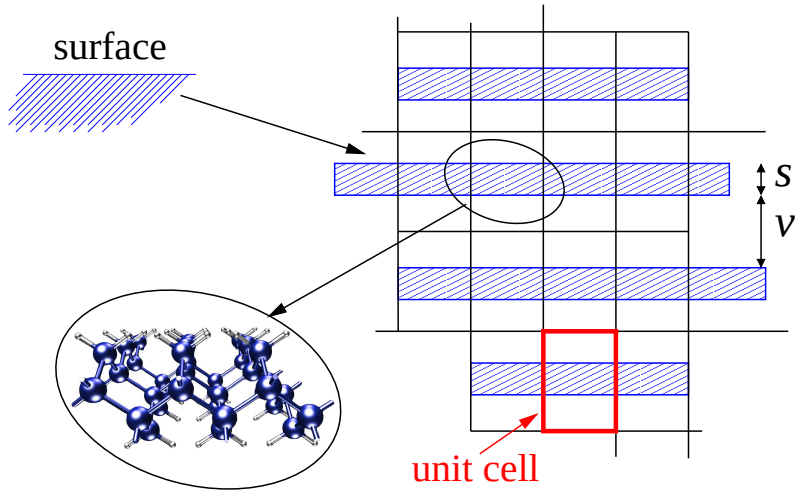

Figure 3.1: The repeated slab approach to describe surfaces.

in Fig. 3.1. The empty region (vacuum) between the individual slabs must thereby be large enough to avoid interactions between the slabs. Since the repeated-slab approach is a structural model, it is conceptually independent of the computational method employed and should work equally well for both DFT-KS and *GW* calculations. However, we will show that the convergence with respect to the basic structural parameters, namely the slab thickness s and the vacuum separation v, depends critically on the underlying physics of each method.

With density functional theory, we seek to determine the electronic ground-state of a neutral[1] system. The slab thickness controls the convergence to the limit of a semi-infinite system, i.e. it is relevant for the description of the substrate for surfaces or supported thin films. It must be thick enough to prevent an interaction of the surfaces across the slab, which depends strongly on the material and the type of the relevant interactions. For metals or other systems with delocalised, free-electron-like electron states, quantisation effects may become important and require large thicknesses, e.g. more than 20 layers for the Al(111) surface [76]. The total energy differences involved are often small ($< 0.1\,\mathrm{eV}$), but the corresponding band structures show larger, sometimes even qualitative changes such as the curvature of the surface resonance at the Γ point for the Si(100) $p(2 \times 1)$ surface [24]. Other important effects include the charge transfer between nonequivalent surfaces, the coupling of surface resonances of opposite surfaces of the slab, or strain. The

[1]Formally charged periodic systems always include a neutralising background charge density.

convergence behaviour for the properties of interest must therefore be tested in each case.

We now come to the coupling between the slabs through the vacuum. As the density decays exponentially in the vacuum region, the direct overlap between the densities of the slabs quickly becomes negligible with increasing separation. Long-range interactions between the slabs can then result only from electrostatic or dispersion interactions. The latter are however not contained in the commonly employed functionals, in particular the LDA. The decay behaviour of the electrostatic interactions along the direction of the broken symmetry z depends on the lowest non-zero multipole moment. The 0th-order moment, i.e. the total charge, vanishes for a neutral system.[2] A non-vanishing 1st-order (dipole) moment requires a "dipole correction" to suppress the intrinsic z^{-1} behaviour [78]. The interaction energy of the 2nd-order (quadrupole) moments decays as z^{-3}, which is sufficient for achieving a fast convergence to the limit of an isolated slab in practice. In summary, the decoupling of uncharged slabs is usually no problematic issue in DFT.

For GW, where we deal with charged excitations and include dynamical polarisation effects, the situation is less favourable. As will be shown next, the long-range tail of the screened interaction must be treated carefully to avoid spurious interactions between quasiparticles and their periodic images. In addition, charged quasiparticles polarise the neighbouring slabs which results in a slowly converging dependence of the quasiparticle energies on the vacuum separation between the slabs. We will show that these long-range effects can be modelled with the classic theory of dielectric screening.

3.2 The long-range tail of W

In this Section the treatment of long-range interaction in GW calculations is discussed. All actual GW implementations involve some approximations for this treatment, the validity of which depends on the physics of the system. In particular, long-range screening in repeated-slab system is inherently anisotropic. It is therefore necessary to review the treatment of the screened interaction for periodic systems in GW. We will do this rather generally and compare to other GW algorithms, too, to show that this issue is intrinsic to GW applied to periodic systems rather than being related to the space-time method or the repeated-slab approach.

[2] We note here that a constant neutralising background charge density for formally charged slab systems varies with the vacuum thickness and introduces again a slow convergence of the total energy and necessitates corresponding corrections [77].

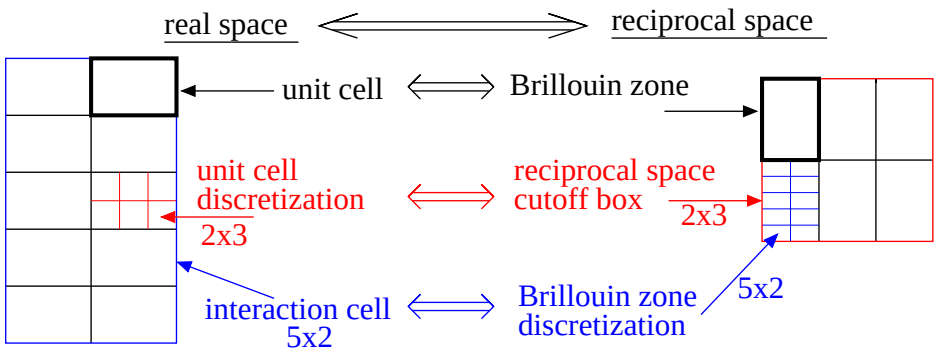

Figure 3.2: Connection between the real and reciprocal space grids. The inner grid in one space corresponds to the outer grid in the other space.

3.2.1 k-point sampling and interaction cell

As an introductory remark, we note that in periodic systems, the two-point functions $F = G$, W, or Σ reflect the lattice periodicity

$$F(\mathbf{r}, \mathbf{r}') = F(\mathbf{r} + \mathbf{R}, \mathbf{r}' + \mathbf{R}) \; . \tag{3.1}$$

We can then introduce the following Wannier-like representation

$$F_{\mathbf{R}}(\mathbf{r}, \mathbf{r}') := F(\mathbf{r} + \mathbf{R}, \mathbf{r}') \; , \tag{3.2}$$

where $\mathbf{r}$ and $\mathbf{r}'$ are restricted to the unit cell. The corresponding Bloch-like representation $F_{\mathbf{k}}$ (also denoted as mixed-space representation [74]) is obtained from a Fourier transformation

$$F_{\mathbf{k}}(\mathbf{r}, \mathbf{r}') := e^{-i\mathbf{k}\cdot(\mathbf{r}-\mathbf{r}')} \sum_{\mathbf{R}} F_{\mathbf{R}}(\mathbf{r}, \mathbf{r}') \, e^{-i\mathbf{k}\cdot\mathbf{R}} \; . \tag{3.3}$$

The reciprocal-space representation is obtained from $F_{\mathbf{k}}$ by Fourier transforming also $\mathbf{r}$ and $\mathbf{r}'$, in full analogy to the plane-wave representation for the lattice-periodic part of a Bloch wavefunction.[3]

$\mathbf{k}$ is a continuous index, which is in practice discretised on a regular, Γ-centred grid ($N_1 \times N_2 \times N_3$) as described in Section 2.2.3. The connection to the Wannier-representation provides us with a real-space picture of this approximation, cf. Fig. 3.2. The Brillouin zone discretisation grid $\mathbf{b}_i/N_i$ is associated with a real space supercell $\mathbf{a}_i \cdot N_i$, i.e. it comprises $N_1 \times N_2 \times N_3$ unit cells. This supercell coincides with the interaction cell of the space-time method, i.e. the range of non-locality for G, W, and Σ [73]. The

[3]Other implementations choose e.g. a Gaussian [79], LMTO [80], or LAPW [81] basis for the lattice periodic part.

discretisation of $\mathbf{k}$ for the function $F_{\mathbf{k}}$ is equivalent to imposing a translational symmetry

$$F_{\mathbf{R}}(\mathbf{r}, \mathbf{r}') = F_{\mathbf{R}+\mathbf{S}}(\mathbf{r}, \mathbf{r}') \,, \tag{3.4}$$

for its Wannier representation, where $\mathbf{S}$ denotes a lattice vector of the interaction cell lattice $(N_i \mathbf{a}_i)$.

We now turn to the effect that the Brillouin zone discretisation has on the two-point functions in a GW calculation. For insulators, the Green's function G decays exponentially for a sufficient separation of its spatial arguments $\mathbf{r}$ and $\mathbf{r}'$ and is essentially zero outside the interaction cell. This behaviour is transferred directly to $P = -iGG$ and $\Sigma = iGW$. For these functions, the Wannier and Bloch representations are numerically equivalent, but this is no longer the case for the slowly decaying bare and screened interaction as we will show next.

3.2.2 The computation of W in reciprocal space

The computation of W from the polarisability P (Eq. 2.50–2.51) is performed in reciprocal space. This has several advantages:

1. The Coulomb potential is diagonal and the real-space convolution becomes a simple multiplication in reciprocal space.

2. The reciprocal-space representation for the lattice-periodic arguments ($\mathbf{G}$ rather than $\mathbf{r}$) is smaller than the corresponding real-space representation when a spherical cutoff is employed.

3. The construction and inversion of the dielectric matrix and the following construction of W can be performed for each $\mathbf{k}$-point separately.

4. The long-range behaviour $\mathbf{R} \to \infty$ is mapped to a finite region in the vicinity of the Γ-point.

While the first two points are specific to plane-wave methods, the other two are independent of the representation of the lattice-periodic arguments. All GW methods with periodic boundary conditions employ the Bloch representation for the construction of W and our considerations apply to all of these. However, we restrict our discussion to plane-wave approaches.

Once W is obtained, the next step is the Fourier transformation to real space in the space-time method, or the reciprocal-space convolution to construct the self-energy matrix elements in reciprocal-space approaches [59, 79, 81]. Both algorithms formally involve an integration over the Brillouin zone, which is replaced by a finite summation over a discrete $\mathbf{k}$-point

grid. As pointed out above, the discretisation corresponds to a periodic repetition in real space, i.e. the outcome of this summation corresponds to a periodic array of quasiparticles instead of an isolated one. When no corrections are applied, the quasiparticle interacts with its periodic images. Since W decays very slowly in real space, the images cannot be simply decoupled by increasing the $\mathbf{k}$-point grid size and the computation becomes numerically unstable. This is most obvious for the $1/r$-part of the screened interaction that gives rise to a divergence of the average potential, which translates to the $1/k^2$ singularity in reciprocal space. This singularity is integrable, i.e. the aforementioned Fourier and convolution integrals are well-defined, but cannot be simply replaced by summations in practice.

That the $1/k^2$ singularity necessitates an explicit treatment has of course been recognised early on [58, 59]. The solution in reciprocal space plane-wave approaches has been to reintroduce the proper integral for the problematic $\mathbf{G} = \mathbf{G}' = \mathbf{0}$ elements. To this end, a model function with the appropriate singularity, for which the integral can be computed analytically, is subtracted from W. The remainder is non-singular and can again be computed by finite summations. After subtraction of the singular function, the $\mathbf{k} = \mathbf{G} = \mathbf{G}' = \mathbf{0}$ element must be set to zero to fix the average potential. The model function is chosen such that the integrals (or approximations to it) can be computed analytically, and a large variety of more or less general models has been proposed [59, 82–85]. In the original space-time method [74], the model function

$$W^{\mathrm{lr,iso}}(\mathbf{k}+\mathbf{G}) = \frac{4\pi\,\overline{\varepsilon}^{-1}}{|\mathbf{k}+\mathbf{G}|^2}\,, \tag{3.5}$$

where $\overline{\varepsilon}$ denotes the average macroscopic dielectric constant, was employed. We have developed a generalisation to treat anisotropic screening to arbitrary precision.[4] We will summarise the most important steps for the treatment of the $1/r$ part in the following section but refer to a recent publication for a discussion of the technical details [86].

3.2.3 Anisotropy in the screened interaction

It can be shown that the head ($\mathbf{G} = \mathbf{G}' = \mathbf{0}$) and the wings ($\mathbf{G} = \mathbf{0}$ or $\mathbf{G}' = \mathbf{0}$) of the dielectric matrix at the Γ-point, i.e., for $\mathbf{k} = \mathbf{0}$, depend on the direction in which the limit $\mathbf{k} \to \mathbf{0}$ is taken [86, 87]. We denote this dependence by the spatial angle $\Omega_{\mathbf{k}}$, and the corresponding normalised direction vector by $\hat{\mathbf{k}}$. To compute this directional limit, a $\mathbf{k}\cdot\mathbf{p}$ perturbation

[4] The treatment of anisotropic screening was jointly developed with Philipp Eggert and Arno Schindlmayr [24, 86].

ansatz is employed, leading to

$$\tilde{\varepsilon}_{\mathbf{00}}(\mathbf{k}, \mathrm{i}\omega) \;\rightarrow\; 1 + \frac{2}{\pi^2} \sum_{\alpha,\beta} \hat{k}_\alpha \hat{k}_\beta \sum_{v,c} \int_{\mathrm{BZ}} \mathrm{d}^3 q \; \frac{\epsilon_{c\mathbf{q}} - \epsilon_{v\mathbf{q}}}{(\epsilon_{c\mathbf{q}} - \epsilon_{v\mathbf{q}})^2 + \omega^2} \times \langle \varphi_{v\mathbf{q}} | r_\alpha | \varphi_{c\mathbf{q}} \rangle \langle \varphi_{c\mathbf{q}} | r_\beta | \varphi_{v\mathbf{q}} \rangle \tag{3.6}$$

and an analogous expression for the wings [86]. α and β are indices for the cartesian components of the vectors $\hat{\mathbf{k}}$ and $\mathbf{r}$. $\epsilon_{n\mathbf{q}}$ and $\varphi_{n\mathbf{q}}$ denote the Kohn-Sham energies and wavefunctions, respectively, and the sum over v (c) runs over occupied (unoccupied) states. The matrix elements of the position operator $\mathbf{r}$ are computed via the commutator with the Hamiltonian and must include the contribution of the non-local pseudopotential for accurate results. In App. E.4, we present an efficient scheme that we have developed for this purpose with an improved scaling behaviour compared to a previous approach [88].

For simplicity, the imaginary frequency argument $i\omega$ is omitted in the following. The directional dependence at the Γ-point is present in the whole inverse dielectric matrix, i.e., head, wings, and body. After block-wise inversion [87] the head of the inverse symmetrised dielectric matrix takes the form

$$\tilde{\varepsilon}^{-1}_{\mathbf{00}}(\Omega_{\mathbf{k}}) = \frac{1}{\hat{\mathbf{k}}^{\mathrm{T}} \mathbf{L} \hat{\mathbf{k}}} \,, \tag{3.7}$$

where the matrix $\mathbf{L}$ is the macroscopic dielectric tensor. We note that in most other implementations where the anisotropy has been considered so far, such as [84, 85], but not Hott [83], the right-hand side of Equation (3.7) was replaced by the expression $\hat{\mathbf{k}}^{\mathrm{T}} \mathbf{L}^{-1} \hat{\mathbf{k}}$ without formal justification.

Combining Equation (3.7) with Equation (2.63), we obtain the head of the screened interaction for $\mathbf{k} \rightarrow \mathbf{0}$

$$W_{\mathbf{00}}(\mathbf{k}) \rightarrow \frac{4\pi}{\mathbf{k}^{\mathrm{T}} \mathbf{L} \mathbf{k}} \,. \tag{3.8}$$

In the space-time method the head of the inverse dielectric matrix is used to define the long-range part of the screened interaction. For this purpose, we extend Equation (3.8) to $\mathbf{G} = \mathbf{G}' \neq \mathbf{0}$ and define the long-range part as

$$W^{\mathrm{lr}}_{\mathbf{G}\mathbf{G}'}(\mathbf{k}) = \frac{4\pi}{(\mathbf{k}+\mathbf{G})^{\mathrm{T}} \mathbf{L} (\mathbf{k}+\mathbf{G})} \delta_{\mathbf{G}\mathbf{G}'} \,. \tag{3.9}$$

The short-range part $W^{\mathrm{sr}} = W - W^{\mathrm{lr}}$ can then safely be Fourier transformed to real space using Fast Fourier Transformations since it is no longer singular. For numerical reasons we subtract the long-range part at the level of the inverse dielectric matrix

$$\tilde{\varepsilon}^{-1,\mathrm{sr}}_{\mathbf{G}\mathbf{G}'}(\mathbf{k}) := \tilde{\varepsilon}^{-1}_{\mathbf{G}\mathbf{G}'}(\mathbf{k}) - \frac{|\mathbf{k}+\mathbf{G}|^2}{(\mathbf{k}+\mathbf{G})^{\mathrm{T}} \mathbf{L} (\mathbf{k}+\mathbf{G})} \delta_{\mathbf{G}\mathbf{G}'} \tag{3.10}$$

and compute W^{sr} from this modified entity according to

$$W^{\mathrm{sr}}_{\mathbf{G}\mathbf{G}'}(\mathbf{k}) = \frac{4\pi}{|\mathbf{k}+\mathbf{G}||\mathbf{k}+\mathbf{G}'|}\tilde{\varepsilon}^{-1,\mathrm{sr}}_{\mathbf{G}\mathbf{G}'}(\mathbf{k}) \ . \tag{3.11}$$

By expanding the angular dependence of W^{lr} into spherical harmonics

$$W^{\mathrm{lr}}_{\mathbf{G}\mathbf{G}'}(\mathbf{k}) = \sum_{l=0}^{\infty}\sum_{m=-l}^{l} H_{lm}\frac{4\pi}{|\mathbf{k}+\mathbf{G}|^2}\delta_{\mathbf{G}\mathbf{G}'}Y_{lm}(\Omega_{\mathbf{k}+\mathbf{G}}) \ , \tag{3.12}$$

we can perform the Fourier transformation of W^{lr} analytically. Only even l contribute to the sum because the coefficients H_{lm} vanish for odd l. The non-vanishing coefficients are obtained by computing the integrals

$$H_{lm} = \int d\Omega_{\mathbf{k}}\ Y^*_{lm}(\Omega_{\mathbf{k}})\frac{1}{\hat{\mathbf{k}}^{\mathrm{T}}\mathbf{L}\hat{\mathbf{k}}} \tag{3.13}$$

numerically on a Lebedev-Laikov angular grid [89]. Making use of the expansion of a plane wave [90] in spherical harmonics Y_{lm} and spherical Bessel functions j_l,

$$e^{i\mathbf{k}\cdot\mathbf{r}} = 4\pi\sum_{l=0}^{\infty}\sum_{m=-l}^{l} i^l j_l(kr)Y_{lm}(\Omega_{\mathbf{r}})Y^*_{lm}(\Omega_{\mathbf{k}}) \tag{3.14}$$

we arrive at

$$W^{\mathrm{lr}}(\mathbf{r},\mathbf{r}') = \sum_{l=0}^{\infty}\sum_{m=-l}^{l} c_l i^l H_{lm}Y_{lm}(\Omega_{\mathbf{r}-\mathbf{r}'})\frac{1}{|\mathbf{r}-\mathbf{r}'|} \ . \tag{3.15}$$

The coefficients c_l for even l are defined as

$$c_l \ = \ \frac{2}{\pi}\int_0^{\infty}\mathrm{d}x\ j_l(x) = \frac{(l-1)!!}{l!!} \tag{3.16}$$

with $n!! = n(n-2)(n-4)\cdots$. In practice we truncate the sum in Equation (3.15) at finite $l = l_{\max} = 4$ as discussed in [86].

For numerical convenience the self energy Σ is split into a static exchange part $\Sigma_{\mathrm{x}} = iGv$ and a frequency-dependent correlation part $\Sigma_{\mathrm{c}} = iG(W-v)$ in the space-time method [74]. We achieve this by subtracting the bare Coulomb interaction v from W^{lr} in its angular expansion (3.12), i.e., we subtract $1/\sqrt{4\pi}$ from H_{00} for each imaginary frequency. Furthermore, the transformation from imaginary frequency to imaginary time is then performed on the expansion coefficients $H_{lm}(\mathrm{i}\omega)$ directly, and we obtain $(W^{\mathrm{lr}}-v)$ according to Equation (3.15) with the expansion coefficients in imaginary time $H_{lm}(\mathrm{i}\tau)$.

A proper treatment of the anisotropy in the long-range part of the screened interaction is crucial to obtain converged results. This is easily illustrated in the space-time method: the density of the **k**-point sampling determines the range of the non-locality in real space. If parts of the long-range interaction remain in W^{sr} for small but finite **k**, then the tails of W^{sr} extend over the boundary of the interaction cell and will be folded back in the numerical Fourier transformation due to the periodic boundary conditions. Since the size of the interaction cell is determined by the **k**-point sampling, an unsatisfactory **k**-convergence behaviour results when the long-range part is treated inadequately.

We have tested this hypothesis with a hydrogen-saturated four layer Si(100) slab [86]. In Figure 3.3 we show the convergence of the quasiparticle energy of the lowest conduction state with respect to the number of **k**-points in the direction perpendicular to the surface. Other states exhibit a similar behaviour. It is obvious that the original isotropic averaging for the screened interaction leads to an unphysical linear increase in the quasiparticle energy. In contrast, the anisotropic treatment converges rapidly. The reason for the linear increase in the isotropic treatment lies in the inadequate treatment of the singularity, which is not fully removed. Integrating $1/|\mathbf{k}|^2$ numerically on a Cartesian grid yields for $k_x = k_y = 0$ with $\Delta k_z = k_{\max}/N_z$

$$\sum_{n=1}^{N_z} \Delta k_z \frac{1}{(n\Delta k_z)^2} \longrightarrow \int_{\Delta k_z}^{k_{\max}} \mathrm{d}k \; \frac{1}{k^2} = \frac{1}{\Delta k_z} - \frac{1}{k_{\max}} = \frac{N_z - 1}{k_{\max}} \tag{3.17}$$

and hence a linearly diverging contribution, whose weight is proportional to $\Delta k_x \Delta k_y \sim (N_x N_y)^{-1}$. When the **k**-sampling is increased in all three directions simultaneously, no such linear divergence occurs, but such a restriction is undesirable and inefficient in practice. Therefore, only the proper anisotropic treatment allows us to investigate the importance of the **k**-point sampling in the direction perpendicular to the surface. To our knowledge, the convergence in the perpendicular direction has not been addressed in previous *GW* calculations for slab systems. We find an $1/N_z$ behaviour the magnitude of which scales as $1/(N_x N_y)$. In the view of the large **k**-point samplings required in the direction parallel to the surface as discussed below, $N_z = 1$ proves to be sufficient in practice.

To summarise, the $1/r$ long-range part of the screened interaction introduces a numerical instability, that can be avoided when appropriate model functions are employed that include the necessary physics. In the space-time approach, the polarisation cloud around each electron is separated into that of a perfectly homogeneous system with the correct average long-range tail and a short-ranged part that contains the microscopic deviations from the

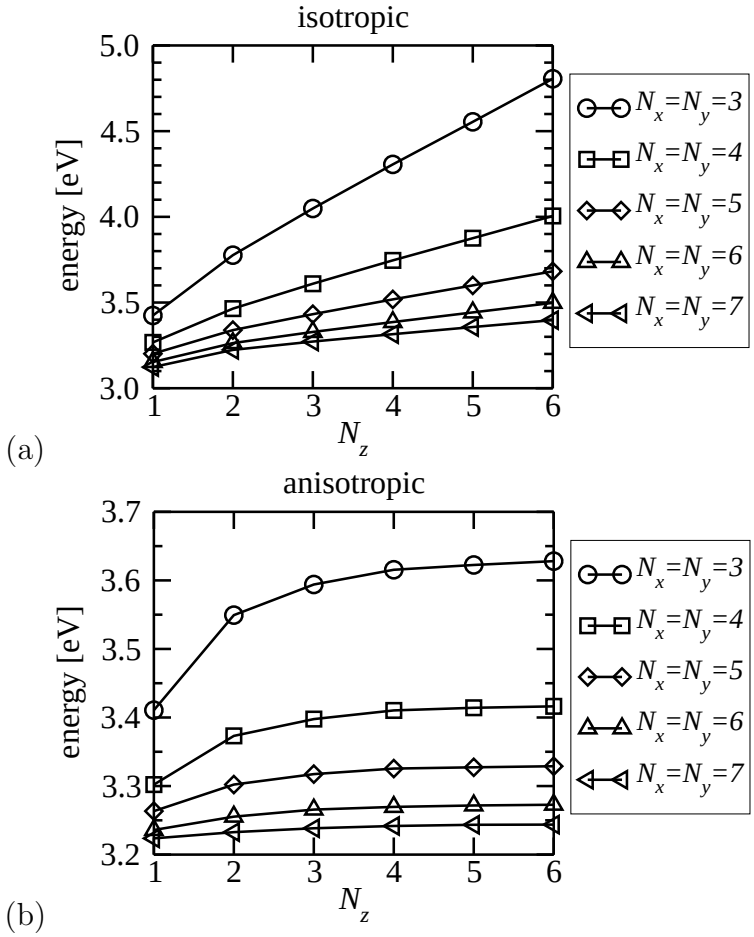

Figure 3.3: Convergence of the lowest conduction-band energy of a Si_4H_4 slab with respect to the number of k-points N_z perpendicular to the surface for (a) the original isotropic implementation and (b) with the anisotropy taken into account. The quantitative behaviour depends on the sampling in the parallel direction ($N_x = N_y$). Note the different scales of the two graphs.

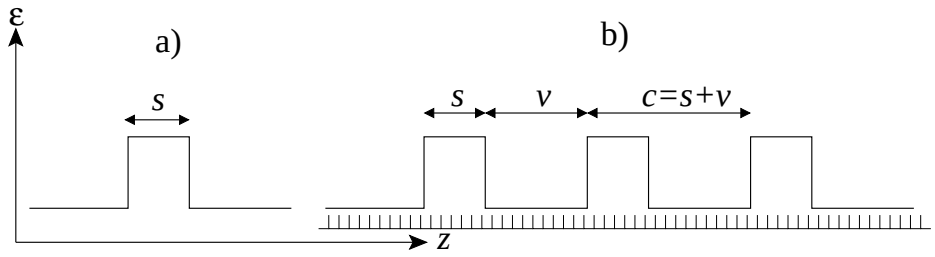

Figure 3.4: Dielectric profiles for a) an isolated slab b) repeated slabs. The discretisation of the z-axis is indicated for the repeated slabs.

average. For slabs, which are inherently anisotropic system, the anisotropy in the screening must be taken into account, and we have presented an efficient formalism for this in the context of the *GW* space-time method.

3.3 Screening in slab systems

In this section, the qualitative features of the screened interaction in isolated and repeated slab systems will be discussed. After describing a simplified dielectric model that reproduces the most important characteristics of the screening, we will discuss its implications for the **k**-point sampling in the parallel direction and the role of the periodic repetition of the isolated slabs.

3.3.1 Dielectric model

In order to learn more about the qualitative behaviour of the screened interaction in a slab system, a dielectric model system is considered in which the slab is modelled as a perfectly homogeneous dielectric medium (dielectric constant ε) with thickness s. The periodic repetition perpendicular to the surface along the z-direction is simulated by a finite number of dielectric slabs, typically 10–20, with a vacuum separation v. We note that s and v are model parameters, but not independent since the total cell height

$$c = s + v \tag{3.18}$$

must agree with that of the full *GW* calculation. In addition to the repeated slabs, we will also discuss the isolated slab as the limiting case for $v \to \infty$. The dielectric profiles $\varepsilon(z)$ for an isolated slab and a repeated slab system are depicted in Fig. 3.4.

For a practical computation of the screened interaction the z-coordinate is discretised, i.e. the slab and the vacuum is partitioned into layers. All layers

have the same thickness and are completely homogeneous. The screened potential is then computed by the method of image charges as described in Section B.1. To this end, we place a unit charge in the centre of a layer z' (an index that we will omit for simplicity in the following). The dielectric discontinuity at the interface to an adjacent layer introduces image charges in both layers. These charges will then induce new image charges due to the next interfaces. In the end, an infinite but discrete set of image charges results from which the screened potential $W(z, \rho)$ in layer z at a lateral separation ρ from the original charge, is computed by[5]

$$W(z, \rho) = \sum_{d=-\infty}^{\infty} \frac{q(z, d)}{\sqrt{d^2 + \rho^2}} \tag{3.19}$$

where $q(z, d)$ are image charges. They depend on the dielectric constants of all layers and the position z' of the original charge.

For the discussion below, we will focus mainly on the image potential, i.e. $z = z'$, $\rho = 0$ and excluding $d = 0$ from the summation. In doing so, we ignore the interplay of quantum effects, which result from the non-locality of the Green's function, with the long-range screening for the quasiparticles. As we will see this is sufficient to develop a qualitative understanding of the additional screening effects in quasiparticle calculations that are introduced when going from a bulk system to a slab system. Two aspects of practical *GW* calculations are well reproduced by the dielectric model:

1. the convergence behaviour with respect to the parallel **k**-point sampling,

2. the convergence behaviour with respect to the vacuum separation in the repeated-slab approach,

and we will discuss these points in the following.

3.3.2 Parallel k-point sampling

In Section 3.2.3 we have shown how to treat the $1/r$-part of the screened interaction by splitting off the macroscopic (average) behaviour. However,

[5]For clarity, we use a slightly different notation here than in Section B.1: here, we include the sign σ into the distance variable d, which can now assume negative values. Also, the dielectric constant of the layer z is absorbed in the image charges, i.e.

$$q(z, d) \hat{=} q(z, d, \sigma)/\varepsilon(z) \; .$$

there may be still interactions that exceed the size of the interaction cell dictated by the **k**-point grid. In bulk systems, the deviations from the average arise mainly from the local variations in the polarisation cloud due to the atomic structure and they usually become negligible when the typical length-scale of these structural variations is exceeded. In a slab system, however, the decisive structural variation is the slab itself and we must expect considerable variations at the length scale of the slab thickness. Usually, the parallel **k**-point sampling of a slab is chosen in analogy to that of the bulk, i.e. sufficiently large to average out the lateral variations in the structure. We can then use the model described above to understand the **k**-point convergence parallel to the slab.

For this purpose we take two essential steps: first we identify the model analogue to the "short-range" part of the screened interaction. We then use the real-space interpretation of a discrete **k**-point sampling, i.e. we take into account a periodic repetition along the ρ-direction parallel to the surface. It is important to clearly distinguish here between the *image charges* and the *periodic images* (cf. Fig. 3.5). The *image charges* are mathematical constructs to compute the screened interaction in our model and are distributed along the z-direction. The *periodic images* are distributed along the ρ-direction and simulate the effect of a discrete **k**-sampling. Since the superposition principle applies, the periodically repeated screened interaction can be computed in our model from the periodic images of the image charges for a single quasiparticle. The periodic repetition in the parallel direction due to the finite **k**-point sampling must also not be mistaken for the periodic repetition in the perpendicular direction in the repeated slab approach. The qualitative parallel behaviour is independent on whether the slabs are repeated or not. We will therefore discuss it for both isolated and repeated slabs.

We assume that in the full G_0W_0 calculation the anisotropic $1/r$ part is taken into account correctly by the long-range treatment of Section 3.2.3. We then have to ask the question how this can be translated to the dielectric model. On this point we note that the image charges $q(z,d)$ become small for large $|d|$ and can be neglected above a certain $d_{\max}$. For $\rho \gg d_{\max}$, we can neglect d in the denominator in Eq. 3.19 and obtain the long-range $1/\rho$ behaviour

$$W^{\mathrm{lr}}(z,\rho) = \frac{q_{\mathrm{eff}}}{\rho} \qquad q_{\mathrm{eff}} = \sum_{d=-d_{\max}}^{d_{\max}} q(z,d)\ . \tag{3.20}$$

The "short-range" part is then obtained as

$$W^{\mathrm{sr}}(z,\rho) \;=\; W(z,\rho) - W^{\mathrm{lr}}(z,\rho)$$

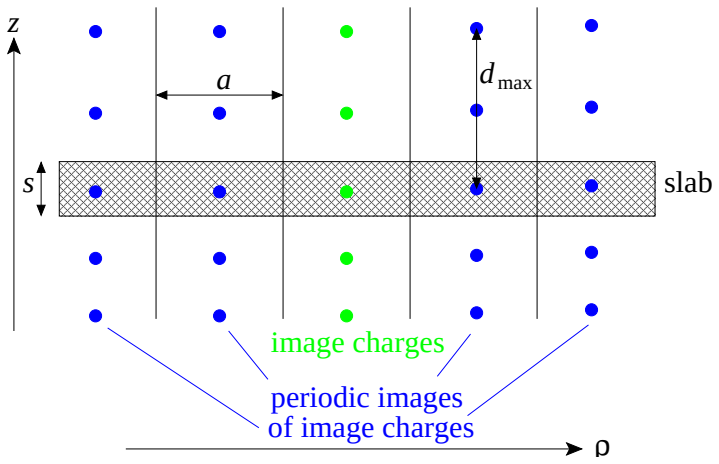

Figure 3.5: Periodic array of image charges to model the artificial periodicity introduced by a finite **k**-sampling, shown schematically for an isolated slab.

$$
\begin{aligned}
&= \sum_{d=-d_{\max}}^{d_{\max}} q(z,d)\left(\frac{1}{\sqrt{d^2+\rho^2}} - \frac{1}{\rho}\right) \\
&= \sum_{d=-d_{\max}}^{d_{\max}} \frac{-q(z,d)d^2}{\rho(\rho+\sqrt{\rho^2+d^2})\sqrt{\rho^2+d^2}} \,. \qquad (3.21)
\end{aligned}
$$

It is this part that remains in the numerical treatment and may not be as short-ranged as the name suggests. The long-range behaviour of W^{sr} is obtained again for $\rho \gg d_{\max}$ and gives

$$
\sum_{d=-d_{\max}}^{d_{\max}} \frac{-q(z,d)d^2}{2\rho^3} \,, \qquad (3.22)
$$

and hence a quadrupolar interaction. Since the average potential is set in the $1/r$ treatment, any shift in the average potential from the quadrupoles is implicitly corrected for.

We will now investigate how the image potential changes when the "short-ranged" part (Eq. 3.21) exceeds the interaction cell for a certain **k**-point sampling in the parallel direction. For this we combine the dielectric model with the idea that a finite **k**-point sampling corresponds to a periodic repetition (cf. Fig. 3.5). We then have to sum the short-range part of the parallel images to obtain the "parallel repetition error" (PRE). For simplicity, we consider only square lattices in the parallel direction. The lattice constant a is related to the number of **k**-points in the parallel direction $N_{\mathbf{k}_\parallel}$ via

$$
a = N_{\mathbf{k}_\parallel} \cdot a_\parallel \,, \qquad (3.23)
$$

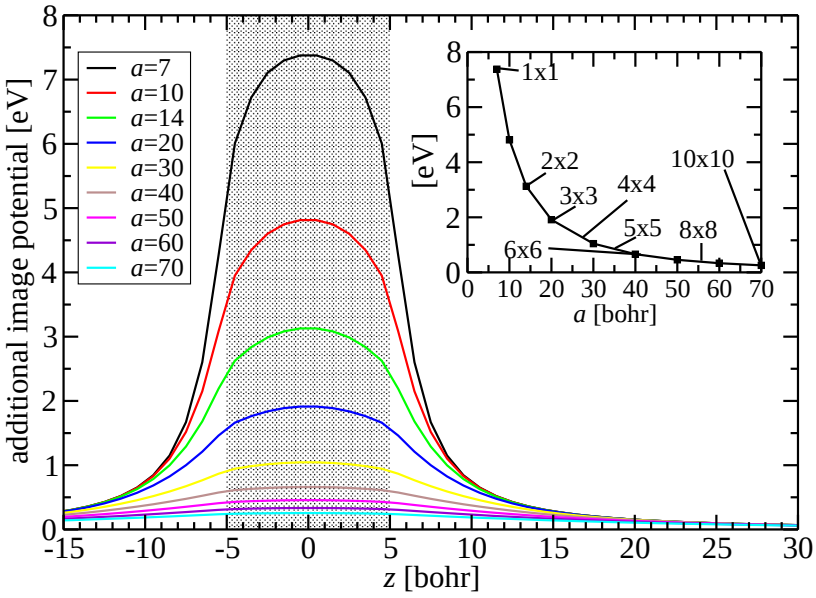

Figure 3.6: Change in the image potential due to a periodic repetition (square lattice, lattice constant a) in the parallel direction. The dielectric model slab (10 bohr thick, $\varepsilon = 2.3$) is indicated by the dotted region and corresponds to a 2-layer NaCl film. The inset shows the value at the centre of the slab as a function of a. The corresponding **k**-sampling ($a_{\parallel} \approx 7\,\text{bohr}$) is also indicated.

where $a_{\parallel}$ is the surface lattice constant of the real systems. The a-dependent change in the image potential from the periodic images then becomes

$$\begin{aligned} \Delta W(z) &= \sum_{n=-\infty}^{+\infty} \sum_{m=-\infty}^{+\infty} W^{\text{sr}}(z, \sqrt{n^2+m^2}\, a) \\ &= \sum_{d=-d_{\max}}^{d_{\max}} q(z,d) \sum_{n,m=-\infty}^{+\infty} \left(\frac{1}{\sqrt{d^2+(n^2+m^2)a^2}} - \frac{1}{\sqrt{n^2+m^2}\, a} \right) \end{aligned} \tag{3.24}$$

excluding $n = m = 0$ from the summation. The sums over n and m are evaluated using the two-dimensional Ewald summation technique.

We first consider an isolated slab with a dielectric constant $\varepsilon = 2.3$, a typical value for NaCl. The influence of the **k**-point sampling on the change in the image potential is investigated by varying the parallel lattice constant a in our model. In Fig. 3.6 it can be seen that the PRE for the image potential is broader than the slab thickness. For small values of a, the effect is very large. With increasing a, the additional image potential quickly becomes smaller and broader. The value at the centre of the slab is then indicative of the magnitude of the PRE within the slab. We will therefore focus on this

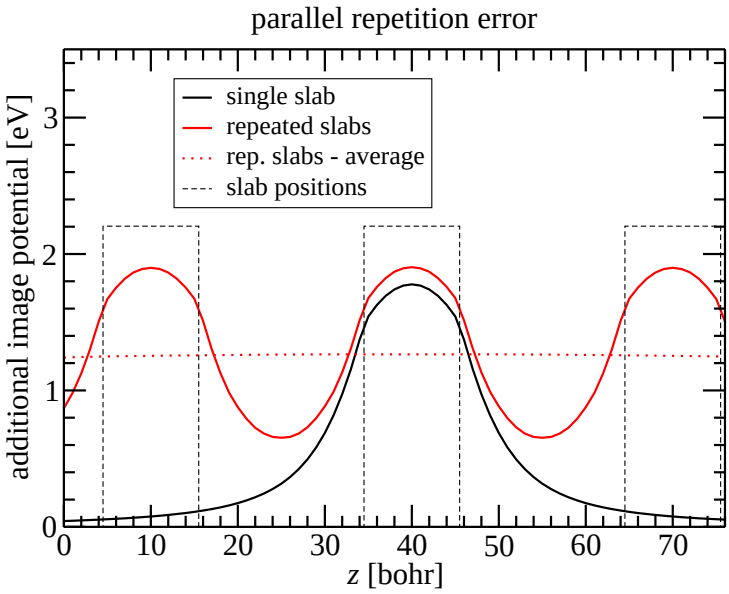

Figure 3.7: Changes in the image potential due to the PRE for an isolated slab and repeated slabs. The model parameters correspond to a 2-layer NaCl slab and a 3×3 **k**-point sampling.

value for the discussing the a-dependence.

We now turn to the periodically repeated slabs. The variation in the image potential for an isolated and a periodically repeated slab is shown in Fig. 3.7. The position of the slabs is indicated by dashed lines. It must be emphasised that the average potential is corrected for during the treatment of the $1/r$ part. This leads to an interesting compensation effect for repeated slabs. The deviation of the additional image potential from its average is much smaller than for an isolated slab.[6] Periodic repetition in the z-direction and small slab separations reduce the error from the parallel **k**-point sampling. We can quantify this by varying the separation between the slabs, shown in Fig. 3.8. The vacuum separation is denoted by the total cell height (i.e. slab + vacuum) for consistency with realistic systems. Increasing the vacuum separation increases the error. The inset demonstrates that also the qualitative convergence behaviour is altered. For large vacuum

[6]The analogue to the average for an isolated slab is the limit $z \to \infty$, which is zero. Only when the isolated slab is placed in a finite cell, an average can be computed. If it is corrected for by setting the $\mathbf{G} = \mathbf{G}' = \mathbf{k} = \mathbf{0}$ element of W^{sr} to zero, the average compensation reduces the PRE for the isolated case, too, but will depend on the cell size. A cell-size dependent parallel convergence has been indeed observed for *GW* calculations where the Coulomb potential has been truncated to decouple neighbouring slabs [25].

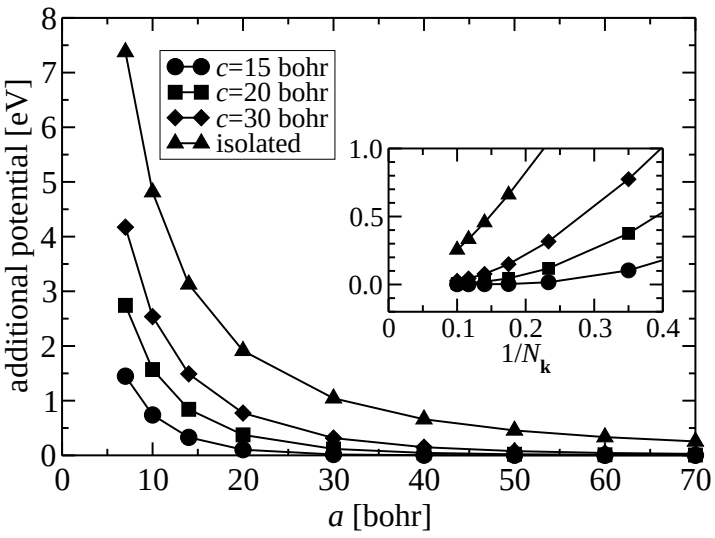

Figure 3.8: Dependence of the PRE at the slab centre on the interaction cell size a for periodically repeated slabs (10 bohr thick, $\varepsilon = 2.3$) with different total cell heights. The isolated slab values are shown for comparison. The inset shows the data as a function of $1/N_{\mathbf{k}}$ for a NaCl slab ($a_{\parallel} = 7$ bohr).

separations or isolated slabs, the error is approximately linear in $1/N_{\mathbf{k}}$ for small values of $N_{\mathbf{k}}$. This dependence becomes increasingly curved when the vacuum separation is decreased, thereby lowering the required **k**-point sampling to achieve a certain accuracy. This is in agreement with Eq. 3.21 that shows a quadrupolar $1/r^3$ behaviour for very large separations, and a $1/r$ for shorter distances. We therefore expect a $1/N_{\mathbf{k}}$ dependence for small $N_{\mathbf{k}}$ and a $1/N_{\mathbf{k}}^3$ for large $N_{\mathbf{k}}$ as the limiting cases.

These qualitative changes have a simple physical reason. The screening in a slab system, which gives rise to the observed behaviour, depends on the length scale. At lateral separations much larger than the slab thickness, we observe an average anisotropic screening with an average dielectric constant $\varepsilon_{\parallel}$ for the parallel direction. This is treated correctly, and the remainder is dominated by the quadrupolar part decaying as $1/r^3$. At lateral separations much smaller than the slab thickness[7] the screening inside the slab is essentially that of the bulk material. The PRE then reflects the difference $(1/\varepsilon - 1/\varepsilon_{\parallel})/r$. In the repeated slab approach, $\varepsilon_{\parallel}$ is the weighted average of the dielectric constant of the bulk and of the vacuum, i.e. the difference between ε and $\varepsilon_{\parallel}$ increases with the vacuum. Small vacuum separations therefore reduce the $1/r$-part of the PRE. This prediction is fully confirmed

[7] or more precisely: the distance from the closest interface

by the convergence behaviour of the quasiparticle energies in repeated slab systems with different amounts of vacuum (e.g. Fig. 3.9).

Unfortunately, the simple models are not sufficient to compute reliable quantitative corrections for the PRE introduced by the finite **k**-sampling. On the one hand, the corrections depend rather sensitively on the model parameters for the dielectric slab, particularly its thickness, and straightforward estimates of the model slab thickness from the dielectric tensor of the repeated-slab system tend to yield overestimated PREs. On the other hand, the additional potential varies over the slab and the COHSEX approach described in Section B.2 may not reduce to a scissors correction.

We can however derive a useful expression for the qualitative convergence behaviour of the quasiparticle energies with respect to the **k**-point sampling. The error in the quasiparticle energy is likely to be proportional to the error in the screened interaction. Assuming that only the closest lateral images play an important role, which is justified by the fast decay of $W^{\mathrm{sr}}(\rho)$, the main effect can be described by a single term in the sum of Eq. 3.24. The proposed fitting function with parameters Q and Z is therefore

$$\Delta E(N_{\mathbf{k}}) = \frac{QZ^2/N_{\mathbf{k}}^3}{1+\sqrt{1+Z^2/N_{\mathbf{k}}^2}+Z^2/N_{\mathbf{k}}^2} \tag{3.25}$$

and turns out to be a reasonable choice. It not only smoothly interpolates between a $1/N_{\mathbf{k}}$ behaviour for small $N_{\mathbf{k}}$ and a $1/N_{\mathbf{k}}^3$ behaviour for large $N_{\mathbf{k}}$ as the limiting cases, but also serves as a robust extrapolation function.

We demonstrate this for NaCl slabs of varying thickness with a $N_{\mathbf{k}}\times N_{\mathbf{k}}\times 1$ sampling in Fig. 3.9. For the 2-layer slab, a large number of **k**-samplings was tested. The good agreement proves that the curvature of the fit function describes the numerical data very well. For thicker slabs there is additional numerical noise, which is however below the expected accuracy of our numerical calculation (0.05 eV). We note also that the vacuum thickness is approximately the same for all slabs. The improvement of the convergence behaviour for thick slabs is therefore exclusively due to the average compensation effects described in this Section. For isolated slabs, the opposite behaviour is expected: thicker slabs should show larger PREs than thin slabs since the closest image charges define the length scale Z for the lateral convergence in Eq. 3.25. This hypothesis can be tested within the dielectric model and is fully confirmed (Fig. 3.10).

It must be emphasised here that the **k**-point sampling has an influence on more than just the long-range part of the screened interaction. Therefore, also other effects contribute to the observed convergence behaviour of the quasiparticle gap. In particular, we observed that the overall convergence

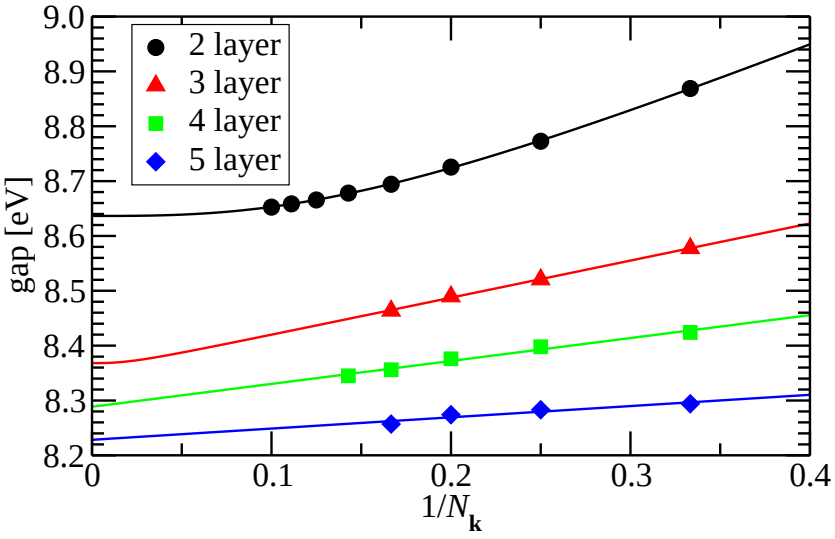

Figure 3.9: **k**-point convergence of the quasiparticle gap for NaCl slabs of varying thickness. The solid lines represent fits to Equation 3.25 (see text).

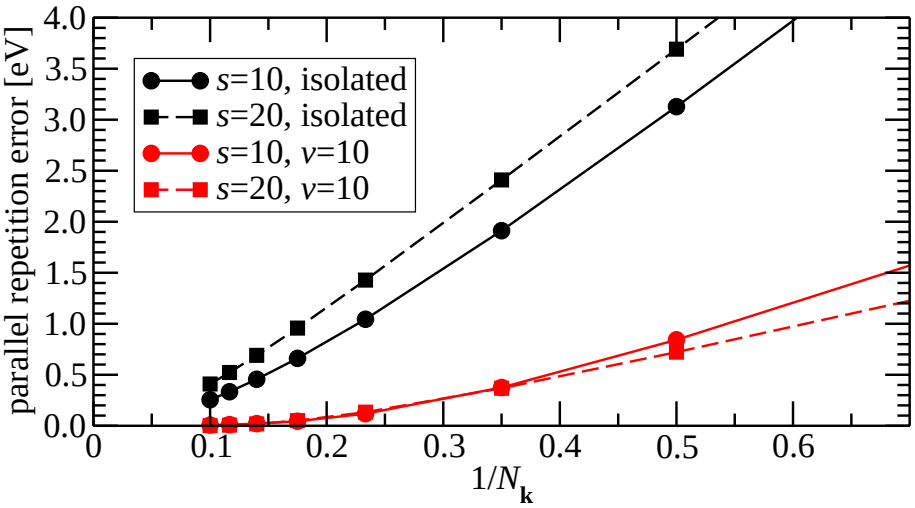

Figure 3.10: Simulated **k**-point convergence behaviour for isolated and periodically repeated (vacuum thickness v=10) slabs (NaCl, $a_{\parallel} = 7$ bohr, ε=2.3) of different thicknesses s. s and v are given in bohr.

with respect to the **k**-sampling orthogonal to the surface depends on the sampling in the parallel direction[8] and becomes very small for sufficiently large **k**-samplings, cf. Fig 3.3. When the convergence in the parallel direction is extrapolated for a fixed sampling in the orthogonal direction, the extrapolated value does practically not depend on the **k**-sampling in the orthogonal direction, i.e. the variation is below the required accuracy. The fitting procedure does therefore also deal with the "under-convergence" in the orthogonal direction.

The qualitative behaviour of the **k**-point convergence described here is not restricted to the *GW* space-time approach. It is an intrinsic property of the reciprocal-space approach for computing the screened interaction when the subsequent Brillouin zone integrals are replaced by summations. We are not aware of an alternative approach in any of the other existing *GW* implementations for periodic systems and would thus assume that these should show a similar behaviour.[9] However, the space-time method may be more appropriate than others to investigate the **k**-point convergence, since the linear scaling of the computation time with respect to the **k**-points is advantageous. The computational effort between the first (3×3) and last point (10×10) of the 2-layer NaCl test increases by a factor of $100/9 \approx 11$ for the space-time method. A convolution approach (i.e. conventional reciprocal-space approaches) scales quadratically with the **k**-point sampling and the last point of the curve would be ∼121 times more expensive to compute than the first point! This may be one of the reasons why the **k**-point convergence behaviour has rarely been addressed for slab systems before [25, 84]. In addition, isotropic screening models for the treatment of the $1/r$ part in the screened interaction do not allow to perform such convergence studies in two dimensions since the errors would introduce a logarithmic divergence similar to the linear divergence that we have demonstrated in Section 3.2.3 for the one-dimensional convergence study.

In summary, the screening in slab system shows specific deviations from the macroscopic $1/r$ behaviour. In the parallel direction, the difference function behaves like $1/r$ for short distances and like $1/r^3$ for longer distances.

[8] It is likely that this is largely due to the neglect of the wing contributions to the Γ-point dielectric matrix.

[9] This may however depend on the details of the implementation. The improved integration technique by Pulci *et al.* [84] for instance is conceptually based on a summation, but employs a modified Coulomb potential which might improve the convergence behaviour in the parallel direction as a side effect. The Coulomb truncation technique of Ismail-Beigi on the other hand includes a different model function for the reciprocal space singularity [25]. Its real-space form is $\beta/\sqrt{\alpha^2 + r^2}$, where α and β are parameters, equivalent to our fitting functions.

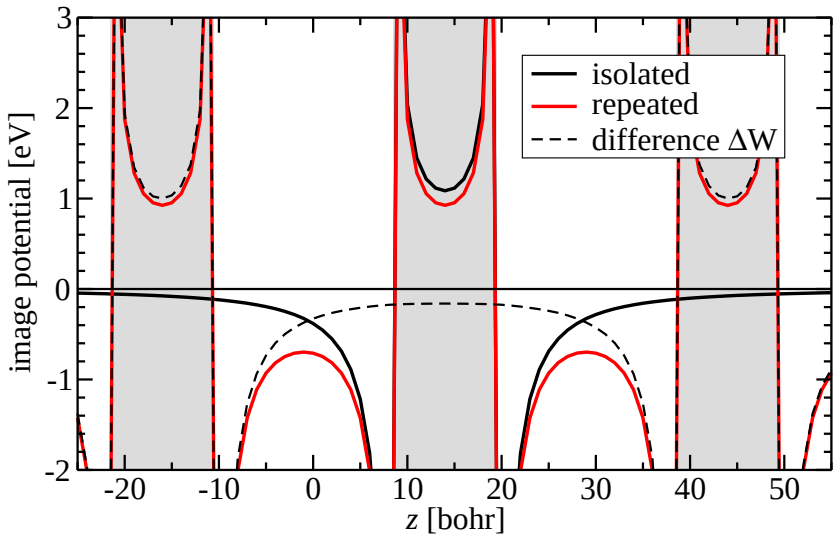

Figure 3.11: Comparison of the image potential for an isolated and a repeated slab (NaCl, ε=2.35, s=11, c=30).

As this difference remains in the numerically treated part of the screened interaction, a peculiar convergence behaviour with respect to the **k**-point sampling parallel to the surface results. The qualitative behaviour can be understood by a simple dielectric slab model. The periodic repetition of the slabs and small vacuum separations reduce this parallel repetition error fortuitously. A robust extrapolation function was derived from the model that can be used to gauge the convergence behaviour with respect to the **k**-point sampling and to extrapolate to the infinite **k**-point limit if necessary.

3.3.3 Periodic repetition in the repeated-slab approach

Until now we have shown how it is possible to obtain numerically converged *GW* results for a repeated slab system, in particular how the description of the long-range interaction must be improved to prevent a coupling between the quasiparticle and its periodic images. However, since we are interested in an isolated thin film or a surface, this is still not the physical system that we want to describe. In other words, the quasiparticle will still see the influence of the periodic images of the slab in the perpendicular direction. When a single quasiparticle is placed in one slab, it will polarise the neighbouring slabs, which will induce a change in the image potential.

It has recently been suggested to prevent this polarisation during the computation by truncating the Coulomb potential [25–27]. All the schemes presented so far truncate v as a function $\mathbf{r} - \mathbf{r}'$ in order to maintain the

reciprocal-space diagonality. To include all interactions with the slab, but to exclude interactions between the slabs, the vacuum thickness must then be (at least) as large as the slab thickness, i.e. the cell size must be twice as large as the slab itself. We argue that this is numerically inefficient. Not only the increased size makes these calculations up to 8 times[10] more expensive than a normal calculation with a small vacuum, but also very large **k**-point samplings may be required for these quasi-isolated slabs as demonstrated above and also found by others [25, 26]. We therefore do not attempt to suppress this effect in the *GW* calculation, but rather correct for it *a posteriori*. The corrections are derived from the dielectric slab model using the dielectric profiles shown in Fig. 3.4. For this purpose, we compute the image potential (without the PRE) for a single slab $W^{\mathrm{iso}}(z)$ and repeated slabs $W^{\mathrm{rep}}(z)$. The resulting image potentials (cf. Fig. 3.11) exhibit non-negligible changes when going from the isolated to the repeated case. However, the difference

$$\Delta W(z) = W^{\mathrm{rep}}(z) - W^{\mathrm{iso}}(z) \tag{3.26}$$

varies very smoothly across the slab [24]. We can therefore apply the simplified COHSEX scheme described in Section B.2 to estimate its contribution to the quasiparticle energies. In this scheme, a constant image potential ΔW would induce a scissor-like change

$$\epsilon^{\mathrm{qp}}(\Delta W) = \epsilon^{\mathrm{qp}}_{\mathrm{iso}} + \begin{cases} +\frac{1}{2}\Delta W & \text{unoccupied} \\ -\frac{1}{2}\Delta W & \text{occupied} \end{cases} \tag{3.27}$$

in the quasiparticle spectrum. We can then correct for instance the quasiparticle gap for this finite-vacuum effect by the change in the image potential, determined at the centre of the (model) slab. In some cases (in particular for surface and image potential states), we may reach the region of non-negligible deviations from the slab centre value. In order to obtain a best guess for the constant part of ΔW we compute its expectation value $\langle\psi_n|\Delta W|\psi_n\rangle$ for each of these states separately.

Since our dielectric layer model (Appendix B.1) allows to compute the image potential for arbitrary dielectric profiles, we are not restricted to integer ratios between vacuum and slab thickness as in previous work in our group [24]. This also poses the question for the optimal model parameters. Assuming the simplest possible model – dielectric slabs with thickness s and

[10] The computational effort scales cubically with the system size when the empty space is covered by basis functions as is the case for plane-waves. The size of the two-point functions then scales quadratically with the system size. The construction of G (space-time approach) or P and Σ (reciprocal-space approaches), that involve a summation over unoccupied states, and the inversion of $\tilde{\varepsilon}$ then scale cubically.

a dielectric constant ε, separated by a vacuum of thickness $c - s$ (where c is the known height of the repeated unit cell), we can link the parallel[11] and orthogonal components of the dielectric tensor $\varepsilon_\parallel$ and ε_z of the repeated slab system to the model parameters via effective medium theory [90]:

$$\varepsilon_\parallel = \frac{(c-s)+\varepsilon s}{c} = 1 + (\varepsilon - 1)\frac{s}{c} \tag{3.28}$$

$$\varepsilon_z^{-1} = \frac{(c-s)+\varepsilon^{-1} s}{c} = 1 - (\varepsilon - 1)\frac{s}{\varepsilon c} \tag{3.29}$$

Solving for ε and s yields

$$\varepsilon = \frac{\varepsilon_\parallel - 1}{1 - \varepsilon_z^{-1}} \tag{3.30}$$

$$s = c \cdot \left[\frac{1}{1-\varepsilon_\parallel} + \frac{1}{1-\varepsilon_z^{-1}}\right]^{-1} \tag{3.31}$$

Since the dielectric tensor is required for the anisotropy treatment, it is computed in the G_0W_0 calculation [86]. Using Eq. 3.30 and 3.31, we can then obtain model parameters for correcting the contribution of the neighbouring slabs to the quasiparticle energies that are consistent with the G_0W_0 calculation. When the thickness of the vacuum is varied, the computed dielectric tensors perfectly agree with the expectations from effective medium theory (not shown here, but in [24]). Correspondingly, the derived model parameters are independent of the vacuum thickness. Moreover, the change in the image potential is not very sensitive to the model parameters, which guarantees a robust correction scheme.

We will now demonstrate that the correction scheme allows to extract the isolated slab quasiparticle energies from a repeated-slab calculation with an arbitrary vacuum thickness. We focus on the quasiparticle gap since the finite vacuum influences mostly the separation between the occupied and unoccupied levels, whereas level shifts within the occupied or unoccupied part of the spectrum due to the weak curvature of ΔW are minor. In Fig. 3.12 we show the results of the **k**-point extrapolation and the resulting gap for a 2-layer NaCl slab with varying amount of vacuum. The graph clearly underlines that for ultrathin slabs, a **k**-point extrapolation for each vacuum separation is crucial to obtain converged results. The convergence behaviour depends on the vacuum thickness, in full agreement with the predictions from Section 3.3. The lower graph on the right shows that the extrapolated quasiparticle correction converges only slowly with increasing cell size to the

[11] possibly averaged

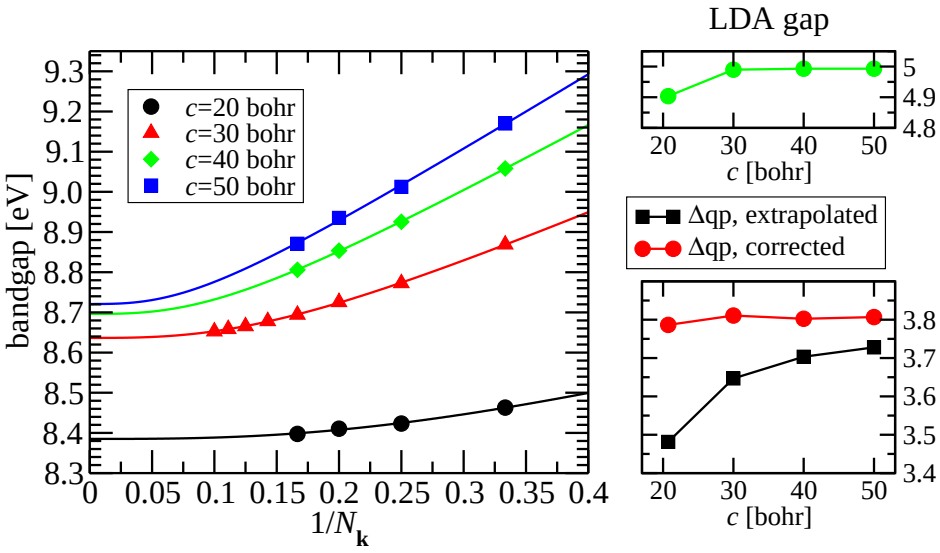

Figure 3.12: Left: **k**-point convergence for the quasiparticle gap of a 2-layer NaCl slab for different total cell heights c. Right: DFT-LDA gap (top) and extrapolated quasiparticle correction Δqp as well as its value corrected for the finite vacuum (bottom) as a function of c.

isolated slab limit. At a finite **k**-point sampling, the increase would be even more dramatic due to the PRE described in the previous section. When the data are corrected for the finite-vacuum effect, however, the quasiparticle correction becomes practically independent of the vacuum thickness. In this very case, the quasiparticle correction including the finite-vacuum correction converges even faster with respect to the vacuum thickness than the underlying LDA calculation. Thus, our *a posteriori* correction even reverses the order of convergence in favour of *GW*.

Earlier results from our group indicated that the dielectric model does not describe the finite-vacuum effect for ultrathin slabs well, which was attributed to the breakdown of a macroscopic description for these systems [24]. We show here that once the **k**-point convergence is carefully extrapolated, the correct physical behaviour is recovered. The success of the modified approach can be attributed to the following improvements:

- The **k**-point convergence is fully taken into account.
- The slab model parameters (thickness and dielectric constant) are extracted from the *GW* calculation and contain possible changes in the dielectric properties of an ultrathin slab.
- The refined dielectric layer model allows to compute the effect for non-

integer vacuum/slab ratios and does not rely on additional interpolation/extrapolation assumptions.

Since the dielectric layer model is not specific to the space-time method, but describes the physical behaviour of repeated slab systems, other *GW* implementations that treat surfaces as periodically repeated slabs must observe the same behaviour. In turn, any implementation that does not recover the slow convergence with respect to the slab separation employs additional implicit or explicit approximations for the long-range behaviour of the screened interaction. We believe that this will in general lead to uncontrollable systematic errors. One example is the treatment of long-range interactions in Rohlfing's Gaussian orbital *GW* implementation [61], which builds – though physically motivated – on assumptions for the screening behaviour at the surface. The improved *GW* space-time method with finite-vacuum corrections yields quasiparticle surface band gaps for semiconductor surfaces which are systematically larger by 0.1 eV to 0.2 eV compared to the Gaussian orbital results [24]. Although other differences between the implementations like the use of plasmon-pole models or the different basis sets might contribute to this discrepancy, the systematic errors due to implicit assumptions increase the theoretical uncertainty considerably compared to the usual estimates of 0.05 eV to 0.1 eV.

3.4 Summary

In this chapter we have reviewed *GW* calculations for two-dimensional systems in the repeated-slab approach. The long-range part of the screened interaction and its role in *GW* calculations were discussed. We have shown that an appropriate treatment of the $1/r$ part is essential to avoid numerical instabilities, and we have presented a treatment that includes anisotropic screening for the space-time method. We have then studied the **k**-point convergence in slab systems, and found that it is dominated by long-range screening effects beyond the anisotropic $1/r$ behaviour. We have proved that the repeated slab approach and *small* vacuum separations are advantageous for this question, and we have developed a reliable and robust extrapolation scheme. Finally, we have demonstrated that the influence of the finite vacuum in the repeated slab approach can be quantitatively corrected for *a posteriori*. It must be emphasised that these issues arise from the construction of the correlation part Σ_c of the self-energy. The exchange self-energy Σ_x and the exchange-correlation potential depend only on the occupied DFT-KS states. Thus, they show essentially the same convergence behaviour as the ground-state calculation [24]. The removal of the self-interaction of the

underlying DFT-LDA calculation is due to these contributions and therefore not affected by the repeated-slab approach. Furthermore, the changes in the self-energy due to the polarisation effects do not vary significantly in the direction parallel to the surface at the length-scale of the unit cell. The corresponding variations of the G_0W_0 corrections to the band structure vary therefore little over the Brillouin zone.[12] We conclude that the combination of an anisotropic treatment, a careful convergence with respect to the **k**-points, and an *a posteriori* correction of the finite-vacuum effect provides an accurate and numerically efficient scheme to compute GW corrections for two-dimensional systems in the repeated-slab approach.

[12]The band structure **k**-point must not be confused with the **k**-point sampling for the construction of Σ. The difference is most obvious in the convolution approach. For a band at point **q** in the Brillouin zone, the relevant self-energy is

$$\Sigma_{\mathbf{q}}(\mathbf{r},\mathbf{r}',i\tau) = \sum_{\mathbf{k}} G_{\mathbf{q}-k}(\mathbf{r},\mathbf{r}',i\tau)W_{\mathbf{k}}(\mathbf{r},\mathbf{r}',i\tau) \ ,$$

where **q** and **k** are independent.